



# Journal of Materials and Engineering Structures

## Research Paper

### Efficient prediction of axial load-bearing capacity of concrete columns reinforced with FRP bars using GBRT model

Xuan-Bang Nguyen <sup>a</sup>, Trong-Ha Nguyen <sup>b</sup>, Kieu-Vinh Thi Nguyen <sup>b</sup>, Thanh-Tung Thi Nguyen <sup>b</sup>, Duy-Duan Nguyen <sup>b,\*</sup>

<sup>a</sup> Institute of Techniques for Special Engineering, Le Quy Don Technical University, Hanoi, Vietnam

<sup>b</sup> Department of Civil Engineering, Vinh University, Vinh 461010, Vietnam

#### ARTICLE INFO

##### Article history:

Received : 19 September 2023

Revised : 26 December 2023

Accepted : 26 December 2023

##### Keywords:

Concrete column reinforced with FRP bars

Axial load-carrying capacity

Gradient boosting regression tree

Graphical user interface

#### ABSTRACT

The behavior of concrete columns reinforced with fiber reinforced polymer (FRP) bars is different from conventional reinforced concrete columns due to the mechanical properties of FRP bars. This study develops a novel machine learning (ML) model, namely gradient boosting regression tree (GBRT), for efficiently predicting the axial load-bearing capacity (ALC) of concrete columns reinforced with FRP bars. A data base containing 283 experimental results is collected to develop the ML model. Seven code-based and empirical-based equations are also included in comparison with the developed ML models. Moreover, we also propose a multiple linear regression (MLR)-based formula for calculating the ALC of the FRP-concrete column. The performance results of GBRT model are compared with those of published formulas and the proposed MLR-based formula. Statistical properties including  $R^2$ , RMSE, and  $a20 - index$  are calculated to evaluate the accuracy of those predictive models. The comparisons demonstrate that GBRT outperforms other models with very high  $R^2$  values and small RMSE. Moreover, the influence of input parameters on the predicted ALC is evaluated. Finally, an efficient graphical user interface tool is developed to simplify the practical design process of FRP-concrete columns.

## 1 Introduction

Reinforced concrete (RC) structures have been degraded their structural capacity due to the reinforcement corrosion. Therefore, it is necessary to prevent the corrosion of reinforcing bars by finding a non-corroded material for reinforcement. Some studies pointed out that fiber reinforced polymer (FRP) bars can be a feasible solution [1, 2]. Previous study showed that flexure and axial theories of RC members are also valid to concrete beams and columns reinforced with FRP bars [3]. However, the design of FRP-concrete components is not just using the conventional formulas since its mechanical properties differ to the normal reinforcement, as illustrated in Fig. 1.

\* Corresponding author,

E-mail address: duyduankxd@vinhuni.edu.vn

Using FRP bars for concrete columns is not specified in ACI 440.1R [4]. Meanwhile, CSA [5] recommends employing FRP bars in concrete columns subjected to centric axial loads, however, the presence of FRP bars in the calculation process is omitted. In the last decades, numerous studies focused on the concrete columns reinforced with FRP longitudinal bars and stirrups[6-10]. Based on those experimental studies, it was pointed out that without consideration of FRP bars underestimates the axial load-bearing capacity (ALC) of columns [10, 11]. Tobbi et al. [10] concluded that the FRP bars contribute a significant role in increasing the axial compression capacity of concrete columns. Elmessalami et al. [12] emphasized that FRP bars can provide from 3%-14% of axial load bearing capacity of columns.

Guidelines for designing FRP-concrete columns under eccentric axial loads are not specified in current design codes such as CSA [5] or ACI 440.1R-15 [4]. However, consideration of the eccentricity in the design process is critical. Thus, it is required to evaluate the column subjected to both axial force and moment. Hadhood et al. [13] tested circular FRP-concrete columns under eccentric loads. They pointed out that glass FRP bars can reach to 0.4% strain at the maximum axial load. Khorramian và Sadeghian [14] concluded that FRP bars were not failed at the maximum compressive loading. Hadi et al. [15] conducted experiments for evaluating the performance of glass FRP-concrete circular columns under centric and eccentric loads. They found that the ALC of columns were reduced when replacing normal reinforcements by FRP bars. A similar observation was also stated in Karim et al. [16]. Moreover, various studies proposed the formulas for calculating ALC of FRP-concrete columns [5-7, 10, 17, 18]. However, the effects of eccentricity have not considered in the previous formulas.

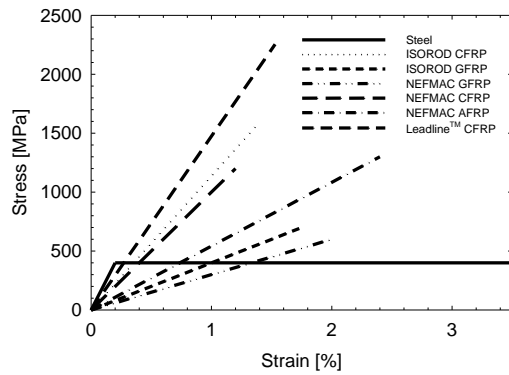


**Fig. 1 – Stress – strain relationship of various FRP bars [19]**

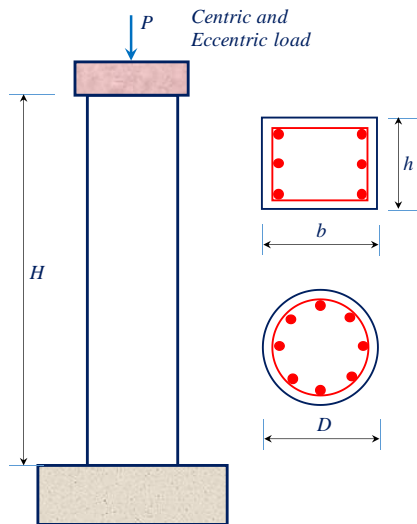


**Fig. 2 – Depiction of tested FRP-concrete columns**

Recently, machine learning (ML) models has been applying popularly in structural engineering [20-24]. Among that, artificial neural network (ANN) is one of the most preferable ML models applying for RC structures [25-36]. Moreover, Genetic algorithm (GA), a type of optimization algorithm, is commonly employed to optimize the weights and biases of the

ANN model and then to improve the prediction accuracy [37–40]. So far, several studies have developed ML models for predicting ALC of FRP-concrete columns. Karimipour et al. [41] developed three ANN models for estimating ALC of concrete columns reinforced with glass FRP bars. They showed that developed ML models outperformed others predictive models with the goodness of fit value ( $R^2$ ) larger than 0.90. Bakouregui et al. [42] presented an extreme gradient boosting model (XGBoost) for predicting ALC of FRP-concrete columns. The performance result of XGBoost algorithm was efficient with  $R^2$  value up to 0.98. Recently, Tarawneh et al. [43] proposed an ANN model for calculating ALC, slenderness ratio as well as developing the interaction diagram of FRC-concrete columns. Cakiroglu et al. [44] developed different ML models to predict the ALC value of concrete columns reinforced with FRP bars. A set of predictive equations was proposed for calculating ALC of the columns. However, it is also required to evaluate the gradient boosting regression tree (GBRT) model for ALC prediction of FRP-concrete columns. Additionally, an efficient tool for simplifying the design process of FRP-concrete columns should be developed.

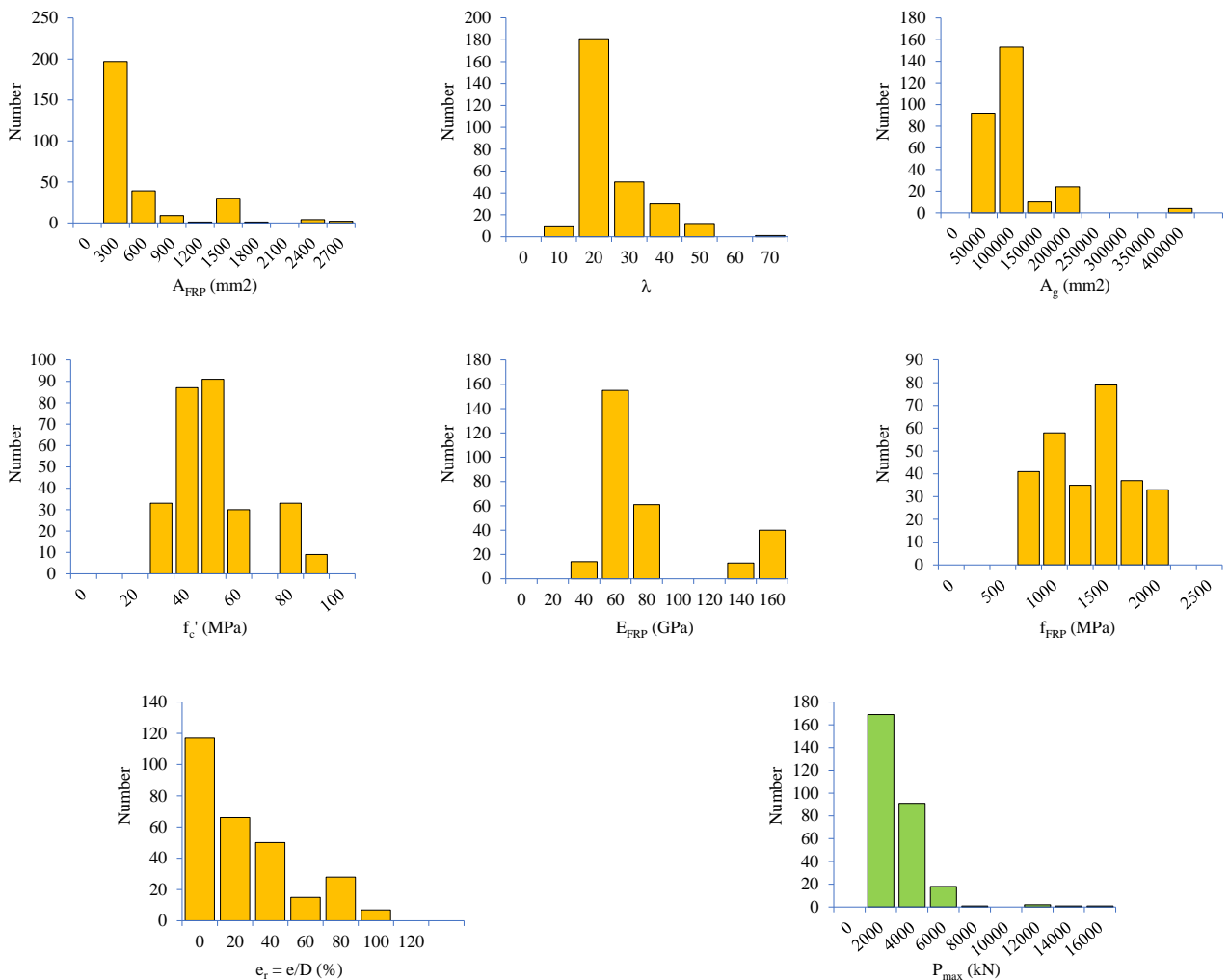


**Fig. 3 – Histograms of the datasets**

This study develops the efficient GBRT model for improving the ALC prediction of FRP-concrete columns. For that, a total of 283 tested specimens of FRP-concrete columns are gathered and employed to develop the ML models. The performance of GBRT is compared with that of seven empirical formulas and a proposed multiple linear regression (MLR)-based formula. Typical statistical properties including  $R^2$ , RMSE, and a20-index are calculated to evaluate the accuracy of those predictive models. Moreover, the effects of input parameters on the predicted ALC are quantified. Finally, a practical graphical user interface (GUI) tool is built for simplifying the design process of the FRP-concrete column.

## 2 Data collection

We collected a set of 283 data sets from published experiments of FRP-RC columns in the literature [6, 7, 10, 13-15, 17, 18, 42, 45-53]. It should be noted that this database considers both rectangular and circular cross-section columns as well as centric and eccentric axial loads. Fig. 2 illustrates the concrete columns reinforced with FRP bars under axial loadings. Table 1 summarizes the used the data samples. Input parameters include the area of the FRP bars ( $A_{FRP}$ ), column slenderness ( $\lambda$ ), gross section area of column ( $A_g$ ), compressive strength of concrete ( $f'_c$ ), elastic modulus of FRP ( $E_{FRP}$ ), ultimate tensile strength of FRP bars ( $f_{FRPu}$ ), and the eccentricity ( $e_r$ ). Whereas  $P_{max}$ , the axial load capacity of columns, is the output parameter. The histogram of the datasets is shown in Fig. 3. Moreover, the correlation between the input and output variables is demonstrated in Fig. 4.

**Table 1 – Statistical indicators of used database**

Parameter	$A_{FRP}$ (mm <sup>2</sup> )	$\lambda$	$A_g$ (mm <sup>2</sup> )	$f'_c$ (MPa)	$E_{FRP}$ (GPa)	$f_{FRPu}$ (MPa)	$e_r = e/D$ (%)	$P_{max}$ (kN)
Min	20	10	14400	26	39	574	0	90
Mean	370	22	75532	45	71	1248	20	2019
Max	2412	62	372100	90	151	2000	100	15235
SD	453	8	50424	14	36	391	25	1867
COV	1.23	0.35	0.67	0.32	0.50	0.31	1.24	0.92

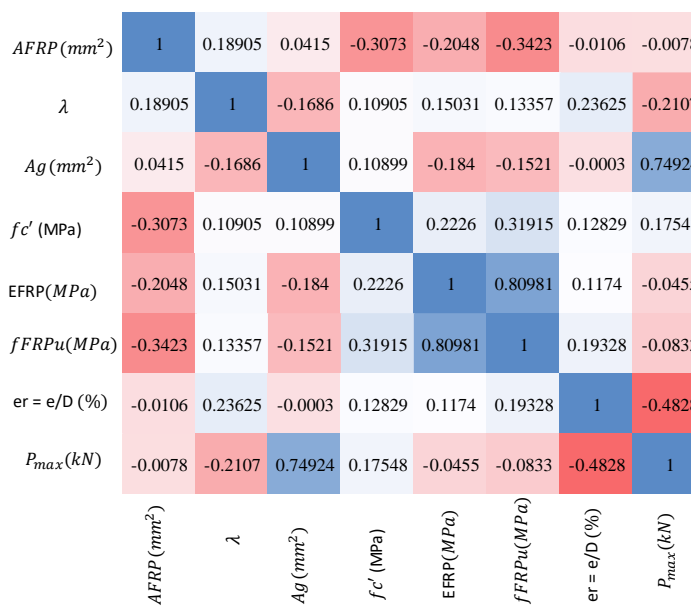


**Fig. 4 – Correlation matrix between the input and output parameters**

## 3 Existing formulas for calculating ALC of FRP-concrete columns

So far, there are numerous studies that proposed equations for calculating the shear strength of FRP-concrete columns. In this study, seven typical formulas are evaluated, including CSA S806-12 [5], Tobbi et al. [10], Affifi et al. [6], Mohamed et al. [7], Maranan et al.[17], Xueet al. [18], and Cakiroglu et al. [44]. Table 2 summarizes the considered published formulas.

**Table 2 -Considered existing formulas for calculating ALC of FRP-concrete columns**

Reference	Formula	
	$P = \alpha_1 f'_c (A_g - A_{FRP})$ ; $\alpha_1 = 0.85$	(1)
CSA S806-12 [5]	$A_g$ is the cross-section area of column; $A_{FRP}$ is the area of FRP bars; $f'_c$ is the compressive strength of concrete.	
Tobbi et al. [10]	$P = \alpha_1 f'_c (A_g - A_{FRP}) + \alpha_{FRP} f_{FRP} A_{FRP}$ ; $\alpha_1 = 0.85$ ; $\alpha_{FRP} = 0.35$	(2)
Affifi et al. [6]	$P = \alpha_1 f'_c (A_g - A_{FRP}) + \alpha_{FRP} f_{FRP} A_{FRP}$ ; $\alpha_1 = 0.85$ ; $\alpha_{FRP} = 0.25$	(3)
Mohamed et al. [7]	$P = \alpha_1 f'_c (A_g - A_{FRP}) + 0.002 E_{FRP} A_{FRP}$ ; $\alpha_1 = 0.85$	(4)
Maranan et al. [17]	$P = \alpha_1 f'_c (A_g - A_{FRP}) + 0.002 E_{FRP} A_{FRP}$ ; $\alpha_1 = 0.9$	(5)
Xue et al. [18]	$P = \alpha_1 f'_c (A_g) + 0.002 E_{FRP} A_{FRP}$ ; $\alpha_1 = 0.85$	(6)
Cakiroglu et al. [44]	$P = 0.00123 A_g^{0.9946} f_c'^{0.9266} \lambda^{-0.1474} \rho_{FRP}^{-0.1474} f_{FRPu}^{0.0589}$ $\rho_{FRP}$ is the longitudinal FRP bar ratio.	(7)

#### 4 Multivariable linear regression (MLR) model

In this study, we propose an equation based on the multivariable regression analysis for calculating ALC of FRP-concrete columns. It should be noted that all input parameters are independent variables, whereas the ALC value is the dependent variable. The general form of multivariable regression is expressed as follows.

$$Y = \beta + a_1 X_1 + a_2 X_2 + a_3 X_3 + \dots + a_n X_n \quad (8)$$

where  $Y$  is the output (i.e., the dependent variable);  $X_1, X_2, \dots, X_n$  are input parameters (i.e., independent variables);  $\beta$  is the coefficient, representing how much  $Y$  is obtained when all  $X_i$  are equal to zero;  $a_1, a_2, \dots, a_n$  regression coefficients. The IBM SPSS Statistics software (ver. 22) is used to develop the multivariable regression equation.

**Table 3 – Results of MLR analysis using SPSS**

Parameter	Regression coefficient		Significance ( <i>p</i> -value)
	Value	Dispersion	
$\beta$	-427.165	268.691	0.113
a1 $A_{FRP}$	0.085	0.116	0.464
a2 $\lambda$	2.36	6.793	0.729
a3 $A_g$	0.029	0.001	0.000
a4 $f'_c$	18.092	3.534	0.000
a5 $E_{FRP}$	8.080	2.237	0.000
a6 $f_{FRPu}$	-0.208	0.222	0.349
a7 $e_r$	-37.575	1.913	0.000
a8 $t_{spacing}$	-1.458	1.057	0.169

Table 3 shows the results of MLR analysis in SPSS, in which all coefficients are shown. It should be noted that the MLR model uses the testing of hypothesis with the *p*-value of 5%. Based on Table 3, it can be found that the gross section

area of column ( $A_g$ ), compressive strength of concrete ( $f'_c$ ), elastic modulus of FRP ( $E_{FRP}$ ), and the eccentricity ( $e_r$ ) have  $p$  values smaller than 0.05. This indicates that those parameters affect the ALC of the column significantly. Finally, the proposed MLR-based formula is expressed as

$$\begin{aligned} P_{max} = & -427.165 + 0.085A_{FRP} + 2.63\lambda + 0.029A_g + 18.092f'_c \\ & + 8.08E_{FRP} - 0.208f_{FRP}u - 37.575e_r - 1.4545t_s \end{aligned} \quad (9)$$

## 5 Development of machine learning models

### 5.1 Gradient boosting regression tree (GBRT) model

GBRT is a prediction algorithm based on a regression model that is widely used in many fields [54-57], it is a combination algorithm of the regression tree algorithm and the gradient-boosting algorithm. It was born to improve the limitations of the two algorithms above [54]. According to [58], GBRT is summarized in the following steps, and a typical flowchart is shown in Fig. 5.

- (1) An initial regression model is created.
- (2) The next regression tree is trained to take the residuals of the previous regression tree.
- (3) Through many iterations, finally obtain a model with high accuracy for prediction results.

The mathematical model of GBRT is shown as follows.

Considering loss function  $L(y, F(x))$ , input dataset  $D = \{(x_1, y_1), \dots, (x_n, y_n)\}$ , and output function values  $F_K(x)$ .

Algorithms:

$$F_0(x) = \underset{h(x)}{\operatorname{argmin}} \sum_{i=1}^n L(y_i, h(x)) \quad (10)$$

For 1 to  $K$

$$F_k(x) = \underset{\gamma}{\operatorname{argmin}} \sum_{i=1}^n L\left(y_i, F_{k-1}(x_i) - \gamma \frac{\partial L(y_i, F_{k-1}(x_i))}{\partial F_{k-1}(x_i)}\right) \quad (11)$$

where

$$F_K(x) = F_{k-1}(x) - \gamma_m \sum_{i=1}^n \nabla_F(y_i, F_{k-1}(x_i)) \quad (12)$$

where  $L(y_i, F(x))$  is loss function,  $D$  is training set,  $(x_1, y_1)$  the first set of data,  $K$  is the number of iterations,  $F_K(x)$  is final model;  $F_k$  is the model after each iteration;  $F_0(x)$  is initial model,  $h(x)$  represents predictions generated by the model;  $\gamma_m$  is the weight of the  $k^{th}$  model.

### 5.2 Performance metrics

To evaluate the optimal model, three performance metrics, which include goodness of fit ( $R^2$ ), root mean squared error ( $RMSE$ ), and  $a20 - index$  are employed to measure the accuracy of the predictive models, as suggested by Zorlu et al. [29]. They are expressed as follows.

$$R^2 = 1 - \left( \frac{\sum_{i=1}^N (t_i - o_i)^2}{\sum_{i=1}^N (t_i - \bar{o})^2} \right) \quad (13)$$

$$RMSE = \sqrt{\left(\frac{1}{n}\right) \sum_{i=1}^n (t_i - o_i)^2} \quad (14)$$

$$a20 - index = \frac{n20}{n} \quad (15)$$

where  $t_i$  and  $o_i$  represent the target and output of  $i^{th}$  data point, respectively;  $\bar{o}$  is the mean of output data samples;  $n$  is the number of samples;  $n20$  is the number of samples with the ratio of the experimental value to the predicted value between 0.8 and 1.0.

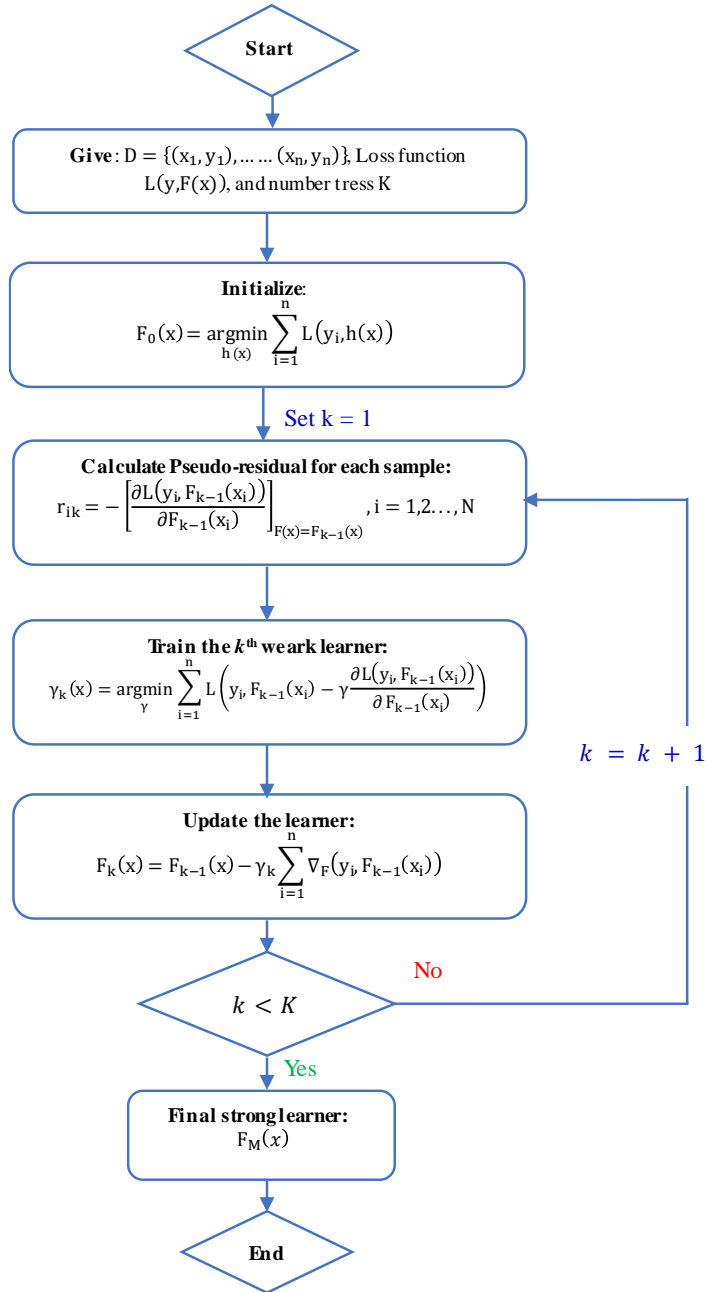


*Fig. 5 – Flowchart of the GBRT model*

## 6 Results and discussion

### 6.1 Performance of GBRT model

The convergence of GA-ANN model was obtained after 1000 iterations and the MSE value was very small, reducing to almost zero after running with 300 trees, as shown in Fig. 6. Additionally, the performance of GBRT is shown in Fig. 7. It can be observed that predicted values are highly matched with those of experiments. This indicates that the GBRT model predicts the ALC of FRP-concrete columns accurately.

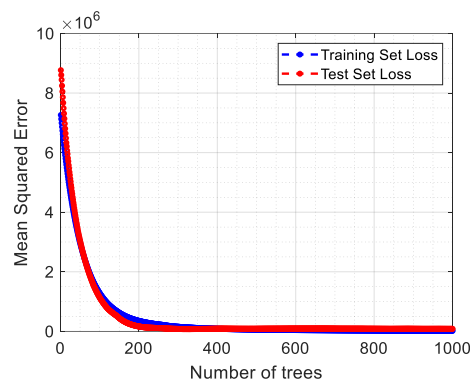


**Fig. 6 – Convergence of GBRT model**

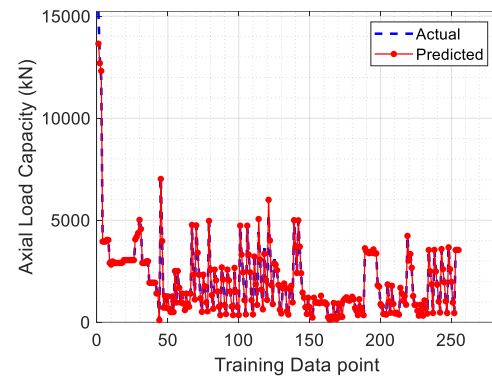


**Fig. 7 – Performance of GBRT model**

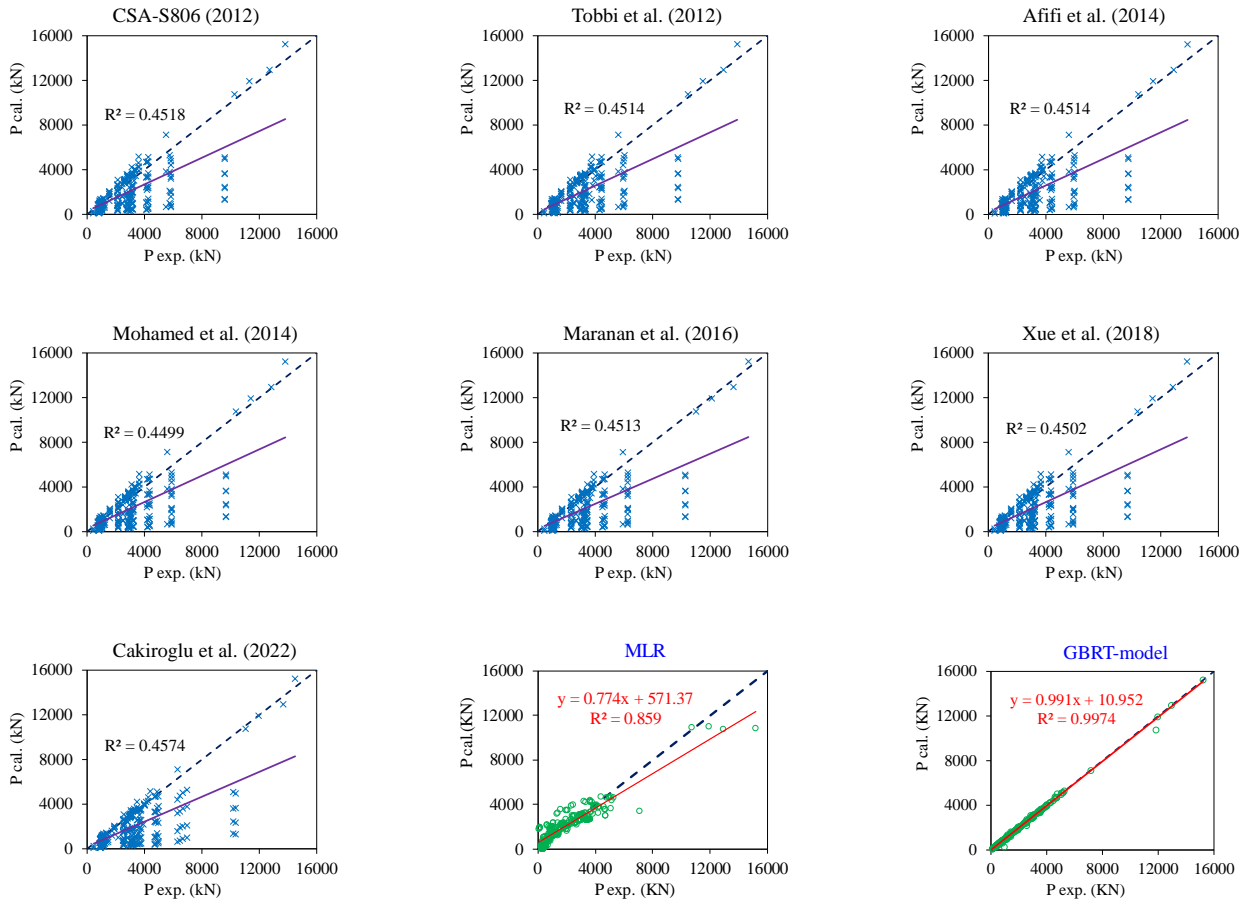


**Fig. 8 – Comparison between the results of considered predictive models**

## 6.2 Comparison between the predictive models

Fig. 8 shows the comparisons of the ALC of FRP-concrete columns between the predictive models and experimental results. It can be found that six empirical-based equations estimate the axial capacity significantly lower compared to that of experiments. In other words, the existing formulas predict the ALC of FRP-concrete columns more conservatively. Moreover, the results obtained from seven previous formulas have a large scattering with a small value of  $R^2$ , approximately 0.45. Even though the recent equation of Cakiroglu et al.[44] included the effects of the slenderness and FRP properties, however the calculated results still had a large difference with the experiments. This discrepancy is likely

due to the effects of eccentricity and elastic modulus of FRP were not considered in the published equations. The proposed MLR-based equation in this study can predict ALC of the column with a high  $R^2$  of 0.857, better than the published ones. Among considered models, the predicted results of GA-ANN and GBRT models are very close to those of experimental ones, in which a small scattering and a very high value of  $R^2$  (0.993 and 0.997, respectively) are obtained.

Fig. 9 compares the calculated statistical indicators for all considered predictive models. Once again, the GBRT model shows a superior performance than the other models. In addition to a higher  $R^2$  value, the  $RMSE$  is also significantly smaller (96 kN) compared to those of previous studies and the proposed MLR-based formulas.

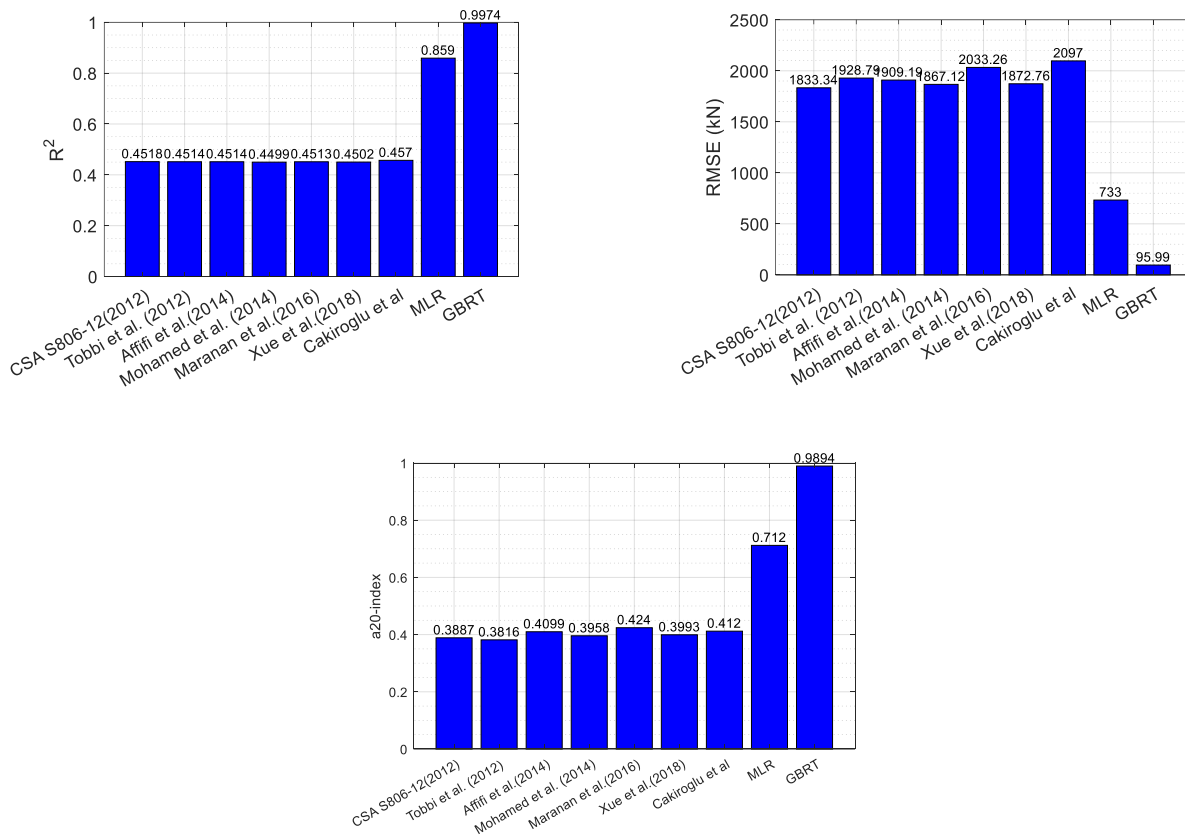


**Fig. 9 – Statistical parameters of various predictive models**

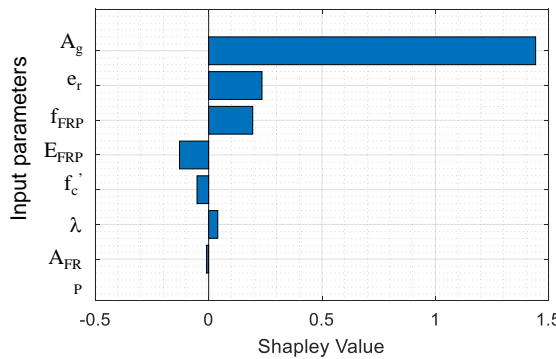


**Fig. 10 – Influence of input parameters on the load-bearing capacity of FRP concrete columns**

### 6.3 Important features

To assess the effects of input parameters on ALC of FRP-concrete columns, a series of sensitivity analyses are performed. In this study, the Shapley value [59] is used to identify the influence of input features on the output. The

Shapley value can help us understand how much each feature or input variable contributed to the final prediction, and how much credit or blame we should assign to each feature for a given prediction. All parameters in Table 1 are considered in calculating Shapley values. The Shapley value result is shown in Fig. 10. It can be found that the gross section area of column ( $A_g$ ) is the most influential parameter on the axial capacity of FRP-concrete columns, followed by the eccentrically ( $e_r$ ) and is the ultimate tensile strength of FRP bars ( $f_{FRPu}$ ).

## 7 Practical GUI tool

To simplify the design process, a practical tool should be developed for rapidly calculating the ALC of FRP-concrete columns. In this study, a graphical user interface (GUI) tool is constructed, in which designers only need to provide input values, then they can immediately obtain the output (i.e., the ACC value). Fig. 11 shows the developed GUI tool using MATLAB. It can be freely access at [https://github.com/duyduan1304/GUI\\_FRP-ConcreteColumn](https://github.com/duyduan1304/GUI_FRP-ConcreteColumn).

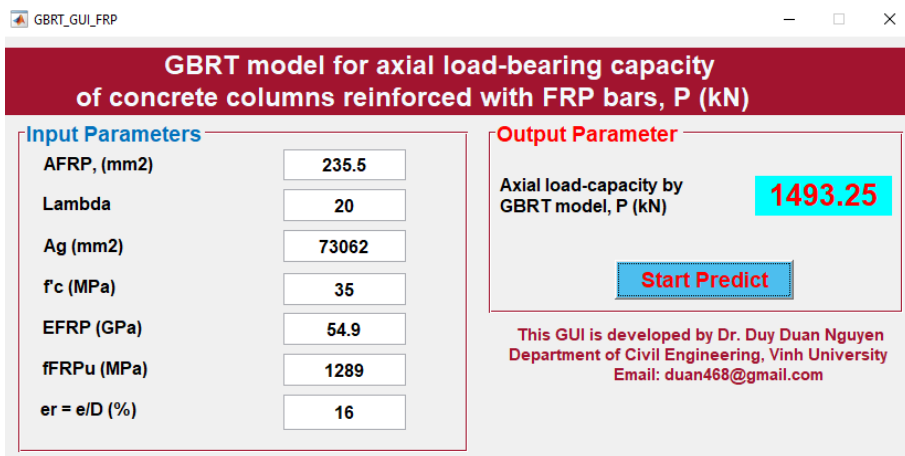


*Fig. 11 – GUI tool*

## 8 Conclusions

This study develops GBRT model for improving the ALC prediction of FRP-concrete columns. A set of 283 experimental data sets of FRP-concrete columns is gathered to construct the ML models. The performance results of GBRT are compared with those of MRL empirical formulas. Statistical parameters including R<sup>2</sup>, RMSE, and a20-index are calculated to evaluate the accuracy of predictive models. The following conclusions are obtained.

The GBRT model accurately predicts the ALC of FRP-concrete columns with a very high R<sup>2</sup> value of 0.997 and small RMSE of 96 kN.

The gross section area of column ( $A_g$ ) is the most influential parameter on the axial capacity of FRP-concrete columns, followed by the eccentrically ( $e_r$ ) and is the ultimate tensile strength of FRP bars ( $f_{FRPu}$ ).

An efficient GUI tool is developed to simplify the design process of FRP-concrete columns.

### Conflicts of interest

The authors declare that they have no potential conflicts of interest in this paper.

### REFERENCES

- [1]- A. Nanni, C. Dolan, Fibre-reinforced-plastic (FRP) reinforcement for concrete structures. Properties and Application, Developments in Civil Engineering. 248p, (1993).
- [2]- B. Tighiouart, B. Benmokrane, D. Gao, Investigation of bond in concrete member with fibre reinforced polymer (FRP) bars. Construction and Building Materials, 12(8) (1998) 453-462.
- [3]- E. Shehata, R. Morphy, S. Rizkalla, Fibre reinforced polymer shear reinforcement for concrete members:

- behaviour and design guidelines. Canadian Journal of Civil Engineering, 27(5) (2000) 859-872.
- [4]- ACI, ACI 440.1 R-15: Guide for the design & construction of structural concrete reinforced with FRP bars, American Concrete Institute Farmington Hills, USA. (2015).
- [5]- CSA, S806-12: Design & Construction of Building Structures with Fibre Reinforced Polymers, Canadian Standards Association Mississauga, Ontario, Canada. (2012).
- [6]- M.Z. Afifi, H.M. Mohamed, B. Benmokrane, Strength and axial behavior of circular concrete columns reinforced with CFRP bars and spirals. Journal of Composites for Construction, 18(2) (2014) 04013035.
- [7]- H.M. Mohamed, M.Z. Afifi, B. Benmokrane, Performance evaluation of concrete columns reinforced longitudinally with FRP bars and confined with FRP hoops and spirals under axial load. Journal of Bridge Engineering, 19(7) (2014) 04014020.
- [8]- O. AlAjarmeh, A. Manalo, B. Benmokrane, W. Karunasena, P. Mendis, K.T. Nguyen, Compressive behavior of axially loaded circular hollow concrete columns reinforced with GFRP bars and spirals. Construction and Building Materials, 194 (2019) 12-23.
- [9]- A. De Luca, F. Matta, A. Nanni, Behavior of full-scale glass fiber-reinforced polymer reinforced concrete columns under axial load. ACI Structural Journal, 107(5) (2010) 589.
- [10]- H. Tobbi, A.S. Farghaly, B. Benmokrane, Concrete Columns Reinforced Longitudinally and Transversally with Glass Fiber-Reinforced Polymer Bars. ACI Structural Journal, 109(4) (2012) 551-558.
- [11]- C.C. Choo, I.E. Harik, H. Gesund, Strength of rectangular concrete columns reinforced with fiber-reinforced polymer bars. ACI Materials Journal, 103(3) (2006) 452.
- [12]- N. Elmessalami, A. El Refai, F. Abed, Fiber-reinforced polymers bars for compression reinforcement: A promising alternative to steel bars. Construction and Building Materials, 209 (2019) 725-737.
- [13]- A. Hadhood, H.M. Mohamed, B. Benmokrane, Strength of circular HSC columns reinforced internally with carbon-fiber-reinforced polymer bars under axial and eccentric loads. Construction and Building Materials, 141 (2017) 366-378.
- [14]- K. Khorramian, P. Sadeghian, Experimental and analytical behavior of short concrete columns reinforced with GFRP bars under eccentric loading. Engineering Structures, 151 (2017) 761-773.
- [15]- M.N. Hadi, H. Karim, M.N. Sheikh, Experimental investigations on circular concrete columns reinforced with GFRP bars and helices under different loading conditions. Journal of Composites for Construction, 20(4) (2016) 04016009.
- [16]- H. Karim, M.N. Sheikh, M.N. Hadi, Axial load-axial deformation behaviour of circular concrete columns reinforced with GFRP bars and helices. Construction and Building Materials, 112 (2016) 1147-1157.
- [17]- G. Maranan, A. Manalo, B. Benmokrane, W. Karunasena, P. Mendis, Behavior of concentrically loaded geopolymmer-concrete circular columns reinforced longitudinally and transversely with GFRP bars. Engineering Structures, 117 (2016) 422-436.
- [18]- W. Xue, F. Peng, Z. Fang, Behavior and Design of Slender Rectangular Concrete Columns Longitudinally Reinforced with Fiber-Reinforced Polymer Bars. ACI Structural Journal, 115(2) (2018).
- [19]- ISIS, ISIS Educational Module 3: An Introduction to FRP-Reinforced Concrete, A Canadian Network of Centers of Excellence ISIS Canada. (2006).
- [20]- A. Kaveh, H. Servati, Design of double layer grids using backpropagation neural networks. Computers & Structures, 79(17) (2001) 1561-1568.
- [21]- A. Kaveh, H.R. Bondarabady, Wavefront reduction using graphs, neural networks and genetic algorithm. International journal for numerical methods in engineering, 60(11) (2004) 1803-1815.
- [22]- A. Kaveh, Y. Gholipour, H. Rahami, Optimal design of transmission towers using genetic algorithm and neural networks. International Journal of Space Structures, 23(1) (2008) 1-19.
- [23]- V.-Q. Nguyen, V.-L. Tran, D.-D. Nguyen, S. Sadiq, D. Park, Novel hybrid MFO-XGBoost model for predicting the racking ratio of the rectangular tunnels subjected to seismic loading. Transportation Geotechnics, 37 (2022) 100878.
- [24]- V.-L. Tran, D.-D. Nguyen, Novel hybrid WOA-GBM model for patch loading resistance prediction of longitudinally stiffened steel plate girders. Thin-Walled Structures, 177 (2022) 109424.
- [25]- D.-D. Nguyen, V.-L. Tran, D.-H. Ha, V.-Q. Nguyen, T.-H. Lee. A machine learning-based formulation for predicting shear capacity of squat flanged RC walls. in: Structures. Elsevier. (2021), 1734-1747. doi:10.1016/j.istruc.2020.12.054.

- [26]- T.-H. Nguyen, N.-L. Tran, D.-D. Nguyen, Prediction of Axial Compression Capacity of Cold-Formed Steel Oval Hollow Section Columns Using ANN and ANFIS Models. *International Journal of Steel Structures*, (2021) 1-26. doi:10.1007/s13296-021-00557-z.
- [27]- T.-H. Nguyen, N.-L. Tran, D.-D. Nguyen, Prediction of Critical Buckling Load of Web Tapered I-Section Steel Columns Using Artificial Neural Networks. *International Journal of Steel Structures*, (2021) 1-23.
- [28]- H. Yang, T. Akiyama, T. Sasaki. A neural network approach to the identification of real time origin-destination flows from traffic counts. in *International Conference on Artificial Intelligence Applications in Transportation Engineering*, 1992, San Buenaventura, California, USA. (1992).
- [29]- K. Zorlu, C. Gokceoglu, F. Ocakoglu, H. Nefeslioglu, S. Acikalin, Prediction of uniaxial compressive strength of sandstones using petrography-based models. *Engineering Geology*, 96(3-4) (2008) 141-158. doi:10.1016/j.enggeo.2007.10.009.
- [30]- V.-L. Tran, S.-E. Kim, Efficiency of three advanced data-driven models for predicting axial compression capacity of CF DST columns. *Thin-Walled Structures*, 152 (2020) 106744. doi:10.1016/j.tws.2020.106744.
- [31]- B. Vakhshouri, S. Nejadi, Prediction of compressive strength of self-compacting concrete by ANFIS models. *Neurocomputing*, 280 (2018) 13-22. doi:10.1016/j.neucom.2017.09.099.
- [32]- M. Rönnholm, K. Arve, K. Eränen, F. Klingstedt, T. Salmi, H. Saxén, ANN modeling applied to NO X reduction with octane. A nn future in personal vehicles, in *Adaptive and Natural Computing Algorithms*. Springer. (2005), 100-103. doi:10.1007/3-211-27389-1\_24.
- [33]- A. Ahmed, S. Elkhatatny, A. Ali, M. Mahmoud, A. Abdulraheem, New model for pore pressure prediction while drilling using artificial neural networks. *Arabian Journal for Science and Engineering*, 44(6) (2019) 6079-6088. doi:10.1007/s13369-018-3574-7.
- [34]- S.S. Selvan, P.S. Pandian, A. Subathira, S. Saravanan, Comparison of response surface methodology (RSM) and artificial neural network (ANN) in optimization of aegle marmelos oil extraction for biodiesel production. *Arabian Journal for Science and Engineering*, 43(11) (2018) 6119-6131. doi:10.1007/s13369-018-3272-5.
- [35]- S.H. Mai, V.-L. Tran, D.-D. Nguyen, V.T. Nguyen, D.-K. Thai, Patch loading resistance prediction of steel plate girders using a deep artificial neural network and an interior-point algorith. *Steel and Composite Structures*, 45(2) (2022) 159.
- [36]- N.-L. Tran, D.-D. Nguyen, T.-H. Nguyen, Prediction of speed limit of cars moving on corroded steel girder bridges using artificial neural networks. *Sadhana*, 47(3) (2022) 1-14.
- [37]- M.A. Bülbül, E. Harirchian, M.F. Işık, S.E. Aghakouchaki Hosseini, E. Işık, A hybrid ANN-GA model for an automated rapid vulnerability assessment of existing RC buildings. *Applied Sciences*, 12(10) (2022) 5138.
- [38]- M. Congro, V.M. de Alencar Monteiro, A.L. Brandão, B.F. dos Santos, D. Roehl, F. de Andrade Silva, Prediction of the residual flexural strength of fiber reinforced concrete using artificial neural networks. *Construction and Building Materials*, 303 (2021) 124502.
- [39]- R. Vijayakumar, N. Pannirselvam, Multi-objective optimisation of mild steel embossed plate shear connector using artificial neural network-integrated genetic algorithm. *Case Studies in Construction Materials*, 17 (2022) e01560.
- [40]- W.B. Chaabene, M.L. Nehdi, Novel soft computing hybrid model for predicting shear strength and failure mode of SFRC beams with superior accuracy. *Composites Part C: Open Access*, 3 (2020) 100070.
- [41]- A. Karimipour, J.M.N. Abad, N. Fasihihour, Predicting the load-carrying capacity of GFRP-reinforced concrete columns using ANN and evolutionary strategy. *Composite Structures*, 275 (2021) 114470.
- [42]- A.S. Bakouregui, H.M. Mohamed, A. Yahia, B. Benmokrane, Explainable extreme gradient boosting tree-based prediction of load-carrying capacity of FRP-RC columns. *Engineering Structures*, 245 (2021) 112836.
- [43]- A. Tarawneh, G. Almasabha, Y. Murad, ColumnsNet: Neural Network Model for Constructing Interaction Diagrams and Slenderness Limit for FRP-RC Columns. *Journal of Structural Engineering*, 148(8) (2022) 04022089.
- [44]- C. Cakiroglu, K. Islam, G. Bekdaş, S. Kim, Z.W. Geem, Interpretable Machine Learning Algorithms to Predict the Axial Capacity of FRP-Reinforced Concrete Columns. *Materials*, 15(8) (2022) 2742.
- [45]- N. ElMessalami, F. Abed, A. El Refai, Response of concrete columns reinforced with longitudinal and transverse BFRP bars under concentric and eccentric loading. *Composite Structures*, 255 (2021) 113057.
- [46]- X. Fan, M. Zhang, Behaviour of inorganic polymer concrete columns reinforced with basalt FRP bars under eccentric compression: An experimental study. *Composites Part B: Engineering*, 104 (2016) 44-56.

- [47]- T.A. Hales, C.P. Pantelides, L.D. Reaveley, Experimental evaluation of slender high-strength concrete columns with GFRP and hybrid reinforcement. *Journal of Composites for Construction*, 20(6) (2016) 04016050.
- [48]- M.N. Hadi, J. Youssef, Experimental investigation of GFRP-reinforced and GFRP-encased square concrete specimens under axial and eccentric load, and four-point bending test. *Journal of Composites for Construction*, 20(5) (2016) 04016020.
- [49]- M. Elchalakani, G. Ma, Tests of glass fibre reinforced polymer rectangular concrete columns subjected to concentric and eccentric axial loading. *Engineering Structures*, 151 (2017) 93-104.
- [50]- M. Guérin, H.M. Mohamed, B. Benmokrane, A. Nanni, C.K. Shield, Eccentric Behavior of Full-Scale Reinforced Concrete Columns with Glass Fiber-Reinforced Polymer Bars and Ties. *ACI Structural Journal*, 115(2) (2018).
- [51]- A. Salah-Eldin, H.M. Mohamed, B. Benmokrane, Structural performance of high-strength-concrete columns reinforced with GFRP bars and ties subjected to eccentric loads. *Engineering Structures*, 185 (2019) 286-300.
- [52]- Z.S. Othman, A.H. Mohammad, Behaviour of eccentric concrete columns reinforced with carbon fibre-reinforced polymer bars. *Advances in Civil Engineering*, 2019 (2019).
- [53]- J. Tu, K. Gao, L. He, X. Li, Experimental study on the axial compression performance of GFRP-reinforced concrete square columns. *Advances in Structural Engineering*, 22(7) (2019) 1554-1565.
- [54]- J.H. Friedman, Greedy function approximation: a gradient boosting machine. *Annals of statistics*, (2001) 1189-1232.
- [55]- X. Hao, X. Hu, T. Liu, C. Wang, L. Wang, Estimating urban PM<sub>2.5</sub> concentration: An analysis on the nonlinear effects of explanatory variables based on gradient boosted regression tree. *Urban Climate*, 44 (2022) 101172. doi:10.1016/j.uclim.2022.101172.
- [56]- C. Qi, A. Fourie, X. Zhao, Back-analysis method for stope displacements using gradient-boosted regression tree and firefly algorithm. *Journal of Computing in Civil Engineering*, 32(5) (2018) 04018031. doi:10.1061/(ASCE)CP.1943-5487.0000779.
- [57]- S. Manna, S. Biswas, R. Kundu, S. Rakshit, P. Gupta, S. Barman. A statistical approach to predict flight delay using gradient boosted decision tree. in 2017 International conference on computational intelligence in data science (ICCIDDS). IEEE. (2017), 1-5. doi:10.1142/S0219691320500277.
- [58]- P. Prettenhofer, G. Louppe. Gradient boosted regression trees in scikit-learn. in PyData 2014. (2014).
- [59]- A.E. Roth, *The Shapley value: essays in honor of Lloyd S. Shapley*. Cambridge University Press, 1988.

## Appendix

The detailed information of the used database.

ID	A <sub>FRP</sub> (mm <sup>2</sup> )	Lamda $\lambda$	Ag (mm <sup>2</sup> )	f' (MPa)	E <sub>FRP</sub> (GPa)	f <sub>FRPu</sub> (MPa)	er = e/D (%)	P <sub>max</sub> (kN)
1	401.92	17	372100	43.7	44.2	608	0	15235
2	401.92	17	372100	40.6	44.4	712	0	12949
3	401.92	17	372100	36.1	44.2	608	0	11926
4	401.92	17	372100	32.8	44.4	712	0	10751
5	2267.08	14	122500	32.6	47.6	728	0	3929
6	2267.08	14	122500	32.6	47.6	728	0	3991
7	2267.08	14	122500	32.6	47.6	728	0	4006
8	2411.52	14	122500	32.6	48.2	751	0	3938
9	2411.52	14	122500	32.6	48.2	751	0	4067
10	157	20	73062	42.9	55.4	934	0	2920
11	78.5	20	73062	42.9	55.4	934	0	2826
12	235.5	20	73062	42.9	55.4	934	0	2998
13	157	20	73062	42.9	55.4	934	0	2857
14	157	20	73062	42.9	55.4	934	0	3019
15	157	20	73062	42.9	55.4	934	0	2964
16	157	20	73062	42.9	55.4	934	0	2804
17	157	20	73062	42.9	55.4	934	0	2951
18	157	20	73062	42.9	55.4	934	0	2865
19	75.36	20	73062	42.9	140	1899	0	2905
20	125.6	20	73062	42.9	140	1899	0	3013
21	125.6	20	73062	42.9	140	1899	0	3107
22	125.6	20	73062	42.9	140	1899	0	2948
23	125.6	20	73062	42.9	140	1899	0	3147
24	125.6	20	73062	42.9	140	1899	0	3070
25	125.6	20	73062	42.9	140	1899	0	2981
26	125.6	20	73062	42.9	140	1899	0	3148
27	125.6	20	73062	42.9	140	1899	0	2941
28	100.48	14	122500	35	46.6	1040	0	3900
29	128.74	14	122500	35	46.3	1040	0	4212
30	226.08	14	122500	35	47.6	728	0	4297
31	200.96	14	122500	35	137	1902	0	5159
32	235.5	14	122500	35	48.2	751	0	4615
33	157	20	73062	42.9	55.4	934	0	2840
34	157	20	73062	42.9	55.4	934	0	2871
35	157	20	73062	42.9	55.4	934	0	2935
36	125.6	20	73062	42.9	140	1889	0	2869
37	125.6	20	73062	42.9	140	1889	0	2960
38	125.6	20	73062	42.9	140	1889	0	3008
39	117.75	16	49087	38	62.6	1184	0	1791
40	117.75	16	49087	38	62.6	1184	0	1981
41	117.75	16	49087	38	62.6	1184	0	1988
42	117.75	16	49087	38	62.6	1184	0	1838
43	117.75	16	49087	38	62.6	1184	0	2063
44	117.75	32	49087	38	62.6	1184	0	1624
45	117.75	32	49087	38	62.6	1184	0	1208
46	19.625	26	14400	34.9	50	1000	67	90
47	19.625	26	14400	34.9	50	1000	17	270
48	117.75	10	73062	90	43	715	0	7126
49	117.75	49	73062	90	43	715	8	3830
50	117.75	49	73062	90	43	715	33	667
51	50.24	13	44100	33.2	67.9	1641	0	1285
52	50.24	13	44100	33.2	67.9	1641	12	803
53	50.24	13	44100	33.2	67.9	1641	24	615
54	75.36	16	33006	37	50	1200	0	1220
55	75.36	16	33006	37	50	1200	12	781
56	75.36	16	33006	37	50	1200	24	494

<b>ID</b>	<b>A<sub>FRP</sub> (mm<sup>2</sup>)</b>	<b>Lamda <math>\lambda</math></b>	<b>A<sub>g</sub> (mm<sup>2</sup>)</b>	<b>f<sub>c'</sub> (MPa)</b>	<b>E<sub>FRP</sub> (GPa)</b>	<b>f<sub>FRPu</sub> (MPa)</b>	<b>er = e/D (%)</b>	<b>P<sub>max</sub> (kN)</b>
57	75.36	16	33006	37	50	1200	0	1309
58	75.36	16	33006	37	50	1200	12	767
59	75.36	16	33006	37	50	1200	24	479
60	75.36	15	34636	85	52	1190	0	2721
61	75.36	15	34636	85	52	1190	12	1599
62	75.36	15	34636	85	52	1190	24	1023
63	75.36	15	34636	85	52	1190	0	2398
64	75.36	15	34636	85	52	1190	12	1572
65	75.36	15	34636	85	52	1190	24	958
66	75.36	16	41600	32.75	46.3	708	0	1366.76
67	75.36	16	41600	32.75	46.3	708	16	880.28
68	75.36	16	41600	32.75	46.3	708	28	584.21
69	75.36	16	41600	32.75	46.3	708	0	1449.06
70	75.36	16	41600	32.75	46.3	708	16	917.16
71	75.36	16	41600	32.75	46.3	708	22	787.8
72	75.36	16	41600	32.75	46.3	708	0	1401.8
73	157	20	73062	70.2	54.9	1289	0	4709
74	157	20	73062	70.2	54.9	1289	8	3309
75	157	20	73062	70.2	54.9	1289	16	2380
76	157	20	73062	70.2	54.9	1289	33	1112
77	157	20	73062	70.2	54.9	1289	66	497
78	235.5	20	73062	70.2	54.9	1289	0	4716
79	235.5	20	73062	70.2	54.9	1289	8	3380
80	235.5	20	73062	70.2	54.9	1289	16	2339
81	235.5	20	73062	70.2	54.9	1289	33	1135
82	235.5	20	73062	70.2	54.9	1289	66	513
83	157	20	73062	35	141	1680	0	3090
84	157	20	73062	35	141	1680	8	2342
85	157	20	73062	35	141	1680	16	1746
86	157	20	73062	35	141	1680	33	995
87	157	20	73062	35	141	1680	66	529
88	157	20	73062	70.2	141	1680	0	5120
89	157	20	73062	70.2	141	1680	8	3671
90	157	20	73062	70.2	141	1680	16	2538
91	157	20	73062	70.2	141	1680	33	1392
92	157	20	73062	70.2	141	1680	66	611
93	157	20	73062	35	54.9	1289	0	2608
94	157	20	73062	35	54.9	1289	8	2134
95	157	20	73062	35	54.9	1289	16	1513
96	157	20	73062	35	54.9	1289	33	745
97	157	20	73062	35	54.9	1289	66	354
98	235.5	20	73062	35	54.9	1289	0	2670
99	235.5	20	73062	35	54.9	1289	8	2123
100	235.5	20	73062	35	54.9	1289	16	1527
101	235.5	20	73062	35	54.9	1289	33	852
102	235.5	20	73062	35	54.9	1289	66	378
103	157	20	73062	35	54.9	1289	0	2564
104	157	20	73062	35	54.9	1289	8	2060
105	157	20	73062	35	54.9	1289	16	1511
106	157	20	73062	35	54.9	1289	33	776
107	157	20	73062	35	54.9	1289	66	366
108	157	20	73062	35.1	54.9	1289	0	2652
109	157	20	73062	35.1	54.9	1289	8	2086
110	157	20	73062	35.1	54.9	1289	16	1483
111	157	20	73062	35.1	54.9	1289	33	747
112	157	20	73062	35.1	54.9	1289	66	355
113	157	20	70686	70.2	141	1680	0	4689
114	157	20	70686	70.2	141	1680	8	3299
115	157	20	70686	70.2	141	1680	17	2435

ID	A <sub>FRP</sub> (mm <sup>2</sup> )	Lamda $\lambda$	A <sub>g</sub> (mm <sup>2</sup> )	f <sub>c'</sub> (MPa)	E <sub>FRP</sub> (GPa)	f <sub>FRPu</sub> (MPa)	e <sub>r = e/D</sub> (%)	P <sub>max</sub> (kN)
116	157	20	70686	70.2	141	1680	33	1045
117	157	20	70686	70.2	141	1680	67	438
118	157	20	70686	70.2	141	1680	0	4680
119	157	20	70686	70.2	141	1680	8	3341
120	157	20	70686	70.2	141	1680	17	2460
121	157	20	70686	70.2	141	1680	33	1061
122	157	20	70686	70.2	141	1680	67	382
123	169.56	17	164025	42.3	51.3	1317	10	4760
124	169.56	17	164025	42.3	51.3	1317	20	3354
125	169.56	17	164025	42.3	51.3	1317	40	1943
126	169.56	17	164025	42.3	51.3	1317	79	745
127	169.56	17	164025	42.3	48.2	838	10	4417
128	169.56	17	164025	42.3	48.2	838	20	3200
129	169.56	17	164025	42.3	48.2	838	40	1589
130	169.56	17	164025	42.3	48.2	838	79	645
131	226.08	17	164025	42.3	51.3	1317	10	5028
132	226.08	17	164025	42.3	51.3	1317	20	3627
133	226.08	17	164025	42.3	51.3	1317	40	2035
134	226.08	17	164025	42.3	51.3	1317	79	914
135	401.92	17	164025	42.3	54.4	1122	10	5294
136	401.92	17	164025	42.3	54.4	1122	20	3790
137	401.92	17	164025	42.3	54.4	1122	40	2110
138	401.92	17	164025	42.3	54.4	1122	79	1008
139	1205.76	21	90000	39	39	654	0	3091
140	1205.76	28	90000	39	39	654	0	2855
141	1205.76	42	90000	39	39	654	0	2411
142	1205.76	21	90000	39	39	654	20	1900
143	1205.76	21	90000	39	39	654	50	647
144	1205.76	21	90000	39	39	654	100	306
145	1205.76	28	90000	39	39	654	20	1702
146	1205.76	35	90000	40.3	39	654	20	1678
147	1205.76	42	90000	40.3	39	654	20	1632
148	1205.76	42	90000	40.3	39	654	50	500
149	1205.76	42	90000	40.3	39	654	100	300
150	803.84	42	90000	40.3	39	654	20	1564
151	2267.08	42	90000	40.3	44	729	20	1823
152	1205.76	42	90000	29.1	39	654	20	1025
153	1205.76	42	90000	55.2	39	654	20	2191
154	169.56	17	160000	71.2	62.7	1236	20	5100
155	169.56	17	160000	71.2	62.7	1236	30	3621
156	169.56	17	160000	71.2	62.7	1236	40	2457
157	169.56	17	160000	71.2	62.7	1236	60	1367
158	169.56	17	160000	71.2	63.7	1646	20	4965
159	169.56	17	160000	71.2	63.7	1646	30	3664
160	169.56	17	160000	71.2	63.7	1646	40	2356
161	169.56	17	160000	71.2	63.7	1646	60	1309
162	75.36	16	41600	26.8	59	930	0	1357
163	75.36	16	41600	26.8	59	930	16	804
164	75.36	16	41600	26.8	59	930	31	454
165	75.36	16	41600	26.8	59	930	47	244
166	75.36	16	41600	26.8	59	930	0	1194
167	75.36	16	41600	26.8	59	930	16	657
168	75.36	16	41600	26.8	59	930	31	353
169	75.36	16	41600	26.8	59	930	47	234
170	75.36	16	41600	26.8	59	930	0	1041
171	452.16	10	40000	25.68	44.25	660	0	970.9
172	452.16	10	40000	25.68	44.25	660	0	951.6
173	452.16	10	40000	25.68	44.25	660	0	937.7
174	314	10	40000	25.68	46	735	0	936.8

ID	A <sub>FRP</sub> (mm <sup>2</sup> )	Lamda $\lambda$	A <sub>g</sub> (mm <sup>2</sup> )	f' <sub>c</sub> (MPa)	E <sub>FRP</sub> (GPa)	f <sub>FRPu</sub> (MPa)	er = e/D (%)	P <sub>max</sub> (kN)
175	615.44	10	40000	25.68	43.75	574	0	981.7
176	452.16	10	40000	25.68	44.25	660	0	954
177	452.16	10	40000	25.68	44.25	660	0	943.2
178	452.16	10	40000	25.68	44.25	660	0	927.7
179	314	35	22500	44.7	150	2000	0	855
180	314	35	22500	44.7	150	2000	50	258
181	314	35	22500	44.7	150	2000	100	119
182	452.16	35	22500	44.7	145	2000	0	909
183	452.16	35	22500	44.7	145	2000	50	262
184	452.16	35	22500	44.7	145	2000	100	126
185	803.84	35	22500	44.7	151	2000	0	960
186	803.84	35	22500	44.7	151	2000	50	290
187	803.84	35	22500	44.7	151	2000	100	137
188	452.16	35	22500	44.7	150	2000	0	899
189	452.16	35	22500	44.7	150	2000	50	264
190	452.16	35	22500	44.7	150	2000	100	129
191	452.16	35	22500	44.7	150	2000	0	925
192	452.16	35	22500	44.7	150	2000	50	237.7
193	452.16	35	22500	44.7	150	2000	100	113
194	678.24	26	41548	25.6	62.3	1113	0	1063
195	904.32	26	41548	25.6	62.3	1113	0	1190
196	1607.68	26	41548	25.6	61.2	1102	0	1227
197	678.24	26	41548	25.6	62.3	1113	0	1065
198	678.24	26	41548	25.6	62.3	1113	0	1085
199	678.24	26	41548	25.6	61.4	1250	0	1055
200	235.5	21	36305	34	59	930	0	943
201	314	21	36305	34	59	930	0	1031
202	392.5	21	36305	34	59	930	0	1286
203	314	21	36305	34	59	930	0	1223
204	314	21	36305	34	59	930	12	846
205	314	21	36305	34	59	930	23	583
206	314	21	36305	34	59	930	35	350
207	314	21	36305	34	59	930	0	1088
208	314	21	36305	34	59	930	12	733
209	314	21	36305	34	59	930	23	538
210	314	21	36305	34	59	930	35	342
211	157	13	73062	46.6	61.8	1449	0	3535
212	157	16	73062	46.6	61.8	1449	0	3490
213	157	23	73062	46.6	61.8	1449	0	3453
214	157	26	73062	46.6	61.8	1449	0	3359
215	235.5	23	73062	46.6	61.8	1449	0	3463
216	235.5	33	73062	46.6	61.8	1449	0	3360
217	339.12	33	73062	46.6	61.7	1411	0	3588
218	157	23	73062	46.6	61.8	1449	0	3417
219	157	33	73062	46.6	61.8	1449	0	3460
220	157	33	73062	46.6	61.8	1449	0	3331
221	157	23	73062	46.6	61.8	1449	16	1807
222	157	33	73062	46.6	61.8	1449	16	1725
223	157	23	73062	46.6	61.8	1449	33	891
224	157	33	73062	46.6	61.8	1449	33	786
225	157	13	73062	46.6	61.8	1449	66	417
226	157	23	73062	46.6	61.8	1449	66	388
227	157	26	73062	46.6	61.8	1449	66	381
228	157	33	73062	46.6	61.8	1449	66	371
229	235.5	23	73062	46	61.8	1449	16	1881
230	235.5	23	73062	46	61.8	1449	33	1029
231	235.5	23	73062	46	61.8	1449	66	448
232	235.5	33	73062	46	61.8	1449	16	1785
233	235.5	33	73062	46	61.8	1449	33	898

ID	A <sub>FRP</sub> (mm <sup>2</sup> )	Lamda $\lambda$	A <sub>g</sub> (mm <sup>2</sup> )	f <sub>c'</sub> (MPa)	E <sub>FRP</sub> (GPa)	f <sub>FRPu</sub> (MPa)	e <sub>r = e/D</sub> (%)	P <sub>max</sub> (kN)
234	235.5	33	73062	46	61.8	1449	66	435
235	339.12	33	73062	46	61.7	1411	66	489
236	157	23	73062	46	61.8	1449	66	420
237	157	33	73062	46	61.8	1449	66	374
238	282.6	17	62730	56.8	43.4	963	23	1480
239	282.6	22	62730	56.8	43.4	963	21	1410
240	169.56	41	62730	56.8	43.4	963	23	1210
241	282.6	41	62730	56.8	43.4	963	21	1315
242	282.6	62	62730	56.8	43.4	963	23	844
243	1205.76	20	98980	37.4	64	1558	0	4224
244	1205.76	20	98980	39.4	64	1558	8	3029
245	1205.76	20	98980	40.7	64	1558	8	3431
246	1205.76	20	98980	38	64	1558	17	2599
247	1205.76	20	98980	37.3	64	1558	34	1278
248	1256	21	32400	28.4	45.9	913	0	879
249	1256	21	32400	28.4	45.9	913	22	518
250	1256	21	32400	28.4	45.9	913	44	315
251	1256	21	32400	28.4	45.9	913	0	792
252	1256	21	32400	28.4	45.9	913	22	520
253	1256	21	32400	28.4	45.9	913	44	324
254	1256	21	32400	28.4	45.9	913	0	875
255	1256	21	32400	28.4	45.9	913	22	568
256	1256	21	32400	28.4	45.9	913	44	334
257	1256	21	32400	34.4	45.9	913	0	1080
258	1256	21	32400	34.4	45.9	913	22	720
259	1256	21	32400	34.4	45.9	913	44	412
260	157	20	73062	52	54.9	1289	0	3530
261	157	20	73062	52	54.9	1289	8	2420
262	157	20	73062	52	54.9	1289	16	1905
263	157	20	73062	52	54.9	1289	33	950
264	157	20	73062	52	54.9	1289	66	440
265	235.5	20	73062	52	54.9	1289	0	3540
266	235.5	20	73062	52	54.9	1289	8	2590
267	235.5	20	73062	52	54.9	1289	16	1775
268	235.5	20	73062	52	54.9	1289	33	1030
269	235.5	20	73062	52	54.9	1289	66	490
270	157	20	73062	52	64.8	1724	0	3530
271	157	20	73062	52	64.8	1724	8	2615
272	157	20	73062	52	64.8	1724	16	1975
273	157	20	73062	52	64.8	1724	33	1015
274	157	20	73062	52	64.8	1724	66	455
275	75.36	20	73062	52	144	1765	0	3705
276	75.36	20	73062	52	144	1765	8	2570
277	75.36	20	73062	52	144	1765	16	1975
278	75.36	20	73062	52	144	1765	33	965
279	75.36	20	73062	52	144	1765	66	445
280	157	20	73062	52	54.9	1289	0	3620
281	117.75	20	73062	52	54.9	1289	0	3340
282	157	20	73062	52	54.9	1289	0	3620
283	157	20	73062	52	54.9	1289	0	3480